AGU PUBLICATIONS

JGR

Journal of Geophysical Research: Oceans

RESEARCH ARTICLE

10.1002/2014JC010350

Key Points:
- Large, nonlinear eddies are detected in the Atlantic Ocean
- The gradient wind balance can be used to describe nonlinear eddies
- Properties of nonlinear eddies can be found from geostrophic velocity fields

Correspondence to:
E. M. Douglass,
elizabeth.douglass.ctr@nrlssc.navy.mil

Citation:
Douglass, E. M., and J. G. Richman (2015), Analysis of ageostrophy in strong surface eddies in the Atlantic Ocean, *J. Geophys. Res. Oceans*, *120*, 1490–1507, doi:10.1002/2014JC010350.

Received 28 JUL 2014
Accepted 14 JAN 2015
Accepted article online 22 JAN 2015
Published online 6 MAR 2015

Analysis of ageostrophy in strong surface eddies in the Atlantic Ocean

E. M. Douglass[1] and J. G. Richman[2]

[1]American Society of Engineering Education, Stennis Space Center, Mississippi, USA, [2]Naval Research Laboratory, Stennis Space Center, Mississippi, USA

Abstract Strongly nonlinear surface eddies are identified and analyzed in a general circulation model. Agulhas rings and Gulf Stream cold-core eddies are examples of eddies that cannot be properly characterized using linear geostrophic dynamics. These eddies are compact, highly circular, persistent in time, and travel long distances while maintaining their characteristics. The nonlinear eddies can be identified by a large Rossby number and high circularity. The majority of the anomalous eddies are anticyclones. Calculation of the balance of forces on these eddies demonstrates that the centrifugal force associated with strong curvature is significant, and the force balance shifts from geostrophy toward a gradient wind balance. Using geostrophy instead of the gradient wind balance produces large errors in estimates of rotational velocity of these eddies. The gradient wind velocity can be calculated from geostrophic velocity and eddy radius. Comparison between the results demonstrates that even when only sea surface height and associated geostrophic velocities are available, strongly nonlinear eddies can be identified and properly characterized. This analysis is then applied to altimetric maps of sea surface height. Nonlinear eddies are present in the altimetric maps, but are less common and not as strongly nonlinear. This analysis demonstrates that by properly accounting for the dynamics of the eddy field, a more complete statistical description including nonlinear terms can be obtained from readily available observations.

1. Introduction/Background

Mesoscale eddies exist everywhere in the world ocean. The geographical distribution of eddies, and a description of their properties, is an important aspect of the global ocean circulation. Most eddies are geostrophic, and as such, can be detected and described by a predictable relationship between rotational speed and sea surface height. This analysis focuses on those eddies which, by virtue of their size and strength of rotation, are not well described by geostrophy. The goal is to detect and describe these eddies only using altimetric maps of sea surface height, since satellite altimetry provides a global data set with good spatial and temporal coverage. The restriction of this analysis to maps of sea surface height does introduce some limitations: submesoscale eddies are too small to be properly described by altimetric maps, for example, and eddies that lack a surface signature are excluded as well. However, the utility of these methods with regard to altimetric maps was one of the primary concerns of the analysis.

Constructing an eddy census (i.e., counting the eddies) is a reasonable method of obtaining a description of the geographical distribution and statistical properties of eddies. There are several methods of detecting and tracking eddies. The present analysis combines two methods to detect robust eddies with signatures in both the velocity and sea surface height fields. With the assumption that eddies are usually geostrophic, a statistical description can be made. While the majority of eddies fit neatly into the description of geostrophic eddies with approximately Gaussian shapes, there are statistical outliers. The outliers display a combination of long lifetime, compact structure, high rotational speed, and large amplitude. These eddies are also highly circular. The intense rotational velocity with relatively short radius leads to a centrifugal force component that alters the balance of forces in these eddies. This effect is particularly strong in some anticyclonic eddies, such as Agulhas rings, and is also noticeable in strong cyclonic features such as Gulf Stream cold-core eddies. While these eddies are few in number, their structure allows them to transport heat and nutrients more efficiently than most other eddies. They also tend to be among the longest-lived and farthest-traveling of the identified eddies.

These strong eddies are the focus of this manuscript. The anticyclonic eddies of note have significantly higher rotational velocities than would be implied from their amplitudes using geostrophy. Thus, they are clearly nonlinear, in the sense that the linear geostrophic relationship between pressure gradients and velocities is not an accurate description of their dynamics. The goal of this analysis is to find a method that identifies these eddies in maps of altimetric height, and accurately describes their properties. This will also quantify the magnitude of the deviation from the a priori assumption of geostrophy in these features. To this end, a set of criteria to evaluate the necessity of applying a correction based on the gradient wind balance is developed. By comparing the results of a sea surface height based analysis with the model's nonlinear velocity field, the accuracy of the correction can be shown. Using these methods, we demonstrate that the nonlinear rotational velocity of a strong eddy can be calculated using only information from sea surface height.

This manuscript is organized as follows: Section 2 contains the model output, and detection and tracking methods. In section 3, we will discuss the quantification of nonlinearity, the choice of nonlinearity parameter, and the prevalence of nonlinearity in the eddy field under consideration. Some examples of these strong, highly nonlinear eddies will also be presented. Section 4 discusses the balance of forces on strongly nonlinear oceanic eddies and the necessity of including the cyclostrophic force. Section 5 discusses the selection criteria of eddies requiring special treatment in their quantification, based on the nonlinearity parameter. Section 6 applies these criteria and analyses to linear geostrophic data to recover the nonlinear eddy velocities. In section 7, the same criteria are applied to eddies detected in AVISO altimetric maps. Finally, there is a summary with some conclusions.

2. Study Setup

2.1. Description of Model Output

This study uses output from a long simulation of HYCOM [*Bleck*, 2002; *Chassignet et al*., 2003; *Halliwell*, 2004]. The details of the model setup used here, along with comparisons of its results to certain regions such as the Indonesia Sea, have been documented in *Metzger et al*. [2010]. The model has 32 hybrid vertical coordinate surfaces with potential density referenced to 2000 m and with a nominal horizontal resolution of 1/12.5° (roughly 8 km at the equator). Since vertical levels are determined by density, there is no straightforward way to choose a depth or number of levels over which to average to approximate an "upper level velocity." Therefore, in the following calculations, only the surface level velocities are used. This is a free-running model with hourly atmospheric forcing from the National Center for Environmental Prediction Climate Forecast System Reanalysis (CSFR) [*Saha et al*., 2010]. Global daily fields of sea surface height and velocity are available. The present analysis focuses on the 3 years from October 2002 to September 2005 in the Atlantic Ocean.

2.2. Detection and Tracking

In essence, two eddy detection methods are used. The first is based on SSH. The details of the SSH method are found in *Chelton et al*. [2011], and only a brief description will be mentioned here. The eddy must be defined by a closed SSH contour, in which the interior extremum is at least 1 cm higher (for anticyclones) or lower (for cyclones) than the enclosing contour. Other criteria include minimum and maximum possible enclosed areas; the minimum is dictated by the resolution of the SSH data set, and the maximum of around 300 km is the maximum size for a feature to be considered "mesoscale" for the purposes of the present analysis.

The second detection method is based on the Okubo-Weiss parameter (W), which is the difference between strain and vorticity:

$$W=\left(\frac{\partial u}{\partial x}-\frac{\partial v}{\partial y}\right)^2+\left(\frac{\partial v}{\partial x}+\frac{\partial u}{\partial y}\right)^2-\left(\frac{\partial v}{\partial x}-\frac{\partial u}{\partial y}\right)^2 \tag{1}$$

In an eddy, vorticity dominates strain, and W is negative. Following previous studies, we define an eddy as an enclosed region with $W = -0.2\sigma$, where σ is the spatial standard deviation of W in the region under consideration [e.g., *Isern-Fontanet et al*., 2003]. Thus, maps of W/σ are searched for closed contours of -0.2, and each of these that meets several other criteria, including minimum and maximum area and velocities that

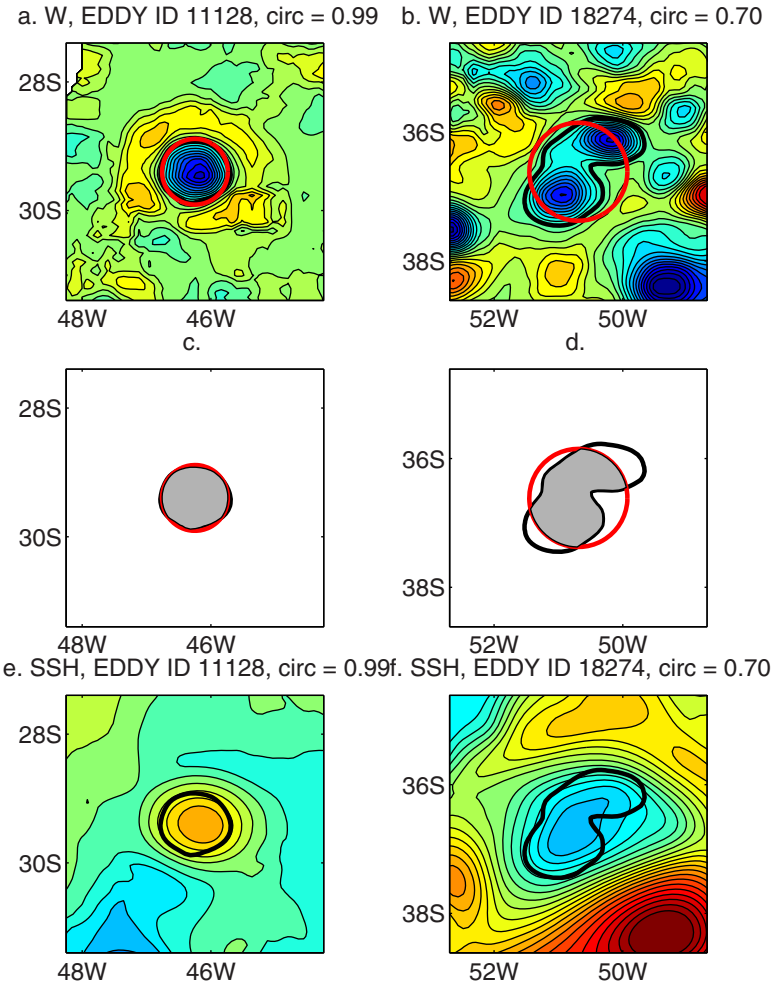

Figure 1. Two eddies, along with the reference circles, demonstrating the "circularity" concept. Eddy borders are shown in black, the reference circles in red. For (a and b), the background field is W/σ, with contour interval of 0.2. (a) Eddy #11128, circularity = 0.99. (b) Eddy #18274, circularity = 0.70. (c and d) The eddy contours from (a and b) (respectively), with their reference circles. The ratio of the shaded area of intersection to the total enclosed contour area is circularity. (e and f) The SSH fields associated with the same eddies.

indicate rotation (both positive and negative u and v velocities), is defined as an eddy. For simplicity, the contour defining the edge of a given eddy will be referred to as the W-contour in the remainder of this manuscript.

For use in the present analysis, eddies must be detected by both of these methods. By this definition, an eddy must be a compact structure with signatures in both SSH and vorticity. This limits overdetection of eddies, and restricts the eddy field to more robust features.

The properties of the eddy are defined following the OW algorithm. It should be noted that descriptions obtained with the SSH algorithm, under the previously noted assumptions of geostrophic eddies with Gaussian shape, are generally consistent with the descriptions from the OW algorithm [*Chelton et al.*, 2011]. The eddy radius (R_{OW}) is defined as the radius of a circle with the area enclosed within the W-contour. Rotational speed (u_{OW}) is calculated from the velocity maps as the average speed along the W-contour.

2.3. Eddy Amplitude

Since the algorithm requires that each eddy have an associated SSH signature, that signature could be used to determine amplitude. However, in order to be consistent with the other parameters, eddy amplitude is first determined following the OW algorithm. We will return to examining the amplitude directly from the SSH field in section 5.1. From the OW algorithm, once rotational speed and radius are determined, two assumptions are necessary to estimate amplitude. The first is that the eddy is in geostrophic balance. In a geostrophic eddy, the velocity is proportional to the gradient of height,

$$fu_R = g\frac{\partial \eta}{\partial r} \tag{2}$$

In this equation, g is the gravitational constant. f is the Coriolis parameter, calculated as a function of latitude. η is the height of the eddy, a function of the radial distance r. u_R is the rotational speed of the eddy. In geostrophic balance, the Coriolis force fu_R is balanced by the pressure gradient force $g\frac{\partial \eta}{\partial r}$.

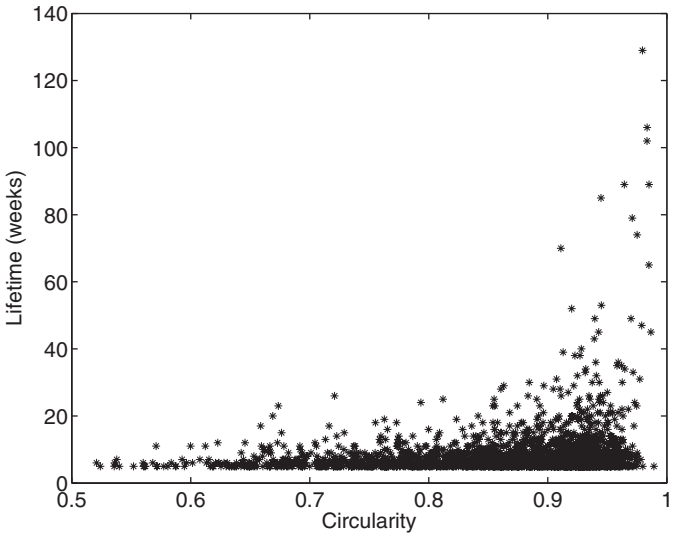

Figure 2. Eddy lifetime in weeks plotted against the eddy's median circularity. Long lifetime only occurs in highly circular eddies.

The second assumption is that the eddy has a Gaussian shape, and a nominal radius R_{OW}. Then, we can estimate the eddy's height at any radius r as:

$$\eta = \eta_0 e^{\frac{-r^2}{2R_{OW}^2}} \quad (3)$$

Using this, we can solve for η_0, the nominal height of a Gaussian eddy with radius R_{OW} and rotational speed u_{OW}:

$$\eta_0 = \frac{f}{g}\frac{u_{OW}}{R_{OW}} e^{1/2} \quad (4)$$

When each eddy is detected, radius and rotational speed are measured, and nominal amplitude is calculated in this way.

2.4. Eddy Circularity

Eddy circularity is also calculated, in order to describe the regularity of the eddy shape. To quantify circularity, for each eddy, a circle with the same center and radius as the eddy is drawn. The ratio of the intersecting area to the total eddy area is the circularity. Examples of circularity are illustrated in Figure 1. Eddy #11128, in Figure 1a, has a circularity of 0.99, while eddy #18724, in Figure 1b, has circularity of 0.70. From the W/σ field, it is clear that eddy #11128 is indeed a single eddy while eddy #18724 shows two eddies, roughly similar to each other in size, enclosed within a single W/σ contour. To calculate circularity, the shaded area in Figures 1c and 1d is divided by the total eddy area. In Figure 1c, the shaded area of intersection is nearly identical to the enclosed area, for a circularity of 0.99, while in Figure 1d the shaded area of intersection is smaller than the total eddy area, indicating lower circularity of 0.70. Low circularity will affect the feature's location, size, and tracking. The shape is thus useful to distinguish between eddies that are similar in other respects. Figures 1e and 1f show the SSH fields associated with the same eddies.

Eddy shape is a particular interest because one of the distinguishing factors of the nonlinear eddies in this analysis is high circularity. While 92% of eddies are found to have circularity higher than 0.7, only 44% of eddies are found to have circularity higher than 0.9. The longest-lived eddies are all found to be highly circular. These eddies may have one or two realizations with low circularity during formation, dissipation, or interactions with other eddies, but the median circularity of long-lived eddies is generally higher than that of shorter-lived eddies. Figure 2 illustrates the connection between high median circularity and high lifetime. High circularity does not necessarily mean a long lifetime, but a long lifetime is always connected with high median circularity. The average lifetime for an eddy with circularity lower than 0.6 is 5.9 weeks. As circularity increases, the average lifetime increases. Eddies with circularity between 0.6 and 0.75 persist for an average of 6.8 weeks, while those with circularity between 0.75 and 0.9 persist for an average of 7.8 weeks. Eddies with circularity over 0.9 have an average lifetime of 11.0 weeks.

2.5. Eddy Tracking

The final step of the algorithm is tracking the eddies. When an eddy is detected, it must be determined if that eddy is newly formed, or if it is a continuation of a previously existing eddy. To that end, the eddy field from the previous week is searched. In order to qualify as a "match," the eddy from the previous week must have the same sense of rotation, amplitude within a factor of 2.5, and center location within three times the radius of the newly detected eddy. If an eddy meeting all these criteria exists, it is considered to be the current eddy's origin. If no such eddies are located, the current eddy is identified as a "new eddy." In this way, each eddy's lifetime is built up one realization at a time. Additionally, translational speed c is estimated by dividing the distance an eddy center moves by the time (one week) for that displacement to occur.

Once the end of the time series is reached, eddies with lifetimes of fewer than 5 weeks (five realizations, with one realization per week) are discarded from the analysis. Thus, persistence is a required element for the inclusion of an eddy in this analysis.

3. Nonlinearity of Eddies

Having identified the physical traits of radius, rotational speed, nominal amplitude, circularity, and lifetime, a remaining challenge is quantifying the nonlinearity of the eddies. As mentioned in section 1, there are several perspectives on what makes an eddy nonlinear. Two methods of quantifying nonlinearity are presented here. The first is the based on the premise that an feature whose rotational speed exceeds its translational speed can trap and transport water, and can thus be described as nonlinear. The second defines linearity as adherence to the linear geostrophic balance, and defines a nonlinear eddy as one for which that balance does not accurately describe the dynamics.

3.1. u_R/c

The ratio of rotational to translational speed (u_R/c) can be used to quantify nonlinearity in eddies [*Chelton et al.*, 2011]. If the eddy is spinning faster than it is translating, it can trap and transport heat, salt, and nutrients within its core. The map of u_R/c (Figure 3a) gives a sense of the patterns of this metric in the Atlantic. The values shown are averages in 1° bins. Fewer than 2% of eddy instances have u_R/c below one, and 65% of eddy instances have u_R/c higher than 5. The map shows high nonlinearity in the Gulf Stream region in the North Atlantic, along the pathway of Agulhas eddies in the south, and across all regions south of 30°S in the Southern Ocean. By this metric, where values higher than one (u_R greater than c) indicate a "nonlinear" eddy, almost all eddies are considered nonlinear.

Instead of simply $u_R/c > 1$, a metric of $u_R/c \gg 1$ could be used to indicate nonlinearity. However, the distribution of u_R/c is quite broad. More than 30% of eddies have u_R/c greater than 10; more than 15% have u_R/c greater than 15, as illustrated in Figure 3c. The quantitative nature of an automatic detection scheme requires the selection of a threshold. With the broad distribution of this metric, it does not seem well suited to this task.

3.2. $|\bar{\omega}/f|$

Another measure of nonlinearity, as mentioned, is the average vorticity over the surface of the eddy ($\bar{\omega}$) normalized by the Coriolis parameter f. This parameter compares the local relative vorticity of the eddy to the planetary vorticity, and is also known as the Rossby number ($|\bar{\omega}/f| = v/fL = Ro$). Since the detection algorithm uses vorticity to locate eddies, it is appropriate to use a parameter with vorticity as a starting point. Figure 3b is a map of $|\bar{\omega}/f|$, averaged into 1° bins. The region from 5°S to 5°N is screened, to eliminate effects from small values of f close to the equator. Patterns of nonlinearity are similar to those from the map of u_R/c, with significant nonlinearity in the Gulf Stream region and in the Southern Ocean. In this map, there is a distinct, very high track of nonlinearity along the track of the Agulhas eddies, and a patch of relatively high nonlinearity in the Gulf Stream. Values in the Southern Ocean are slightly elevated but not excessively so. There is also high nonlinearity in the tropics near the coast of south and central America, which could be a signature of North Brazil Current retroflection rings, or could be related to low values of the Coriolis parameter f. However, the overall average nonlinearity values are below 0.2 in most regions, indicating that the region is generally linear with respect to geostrophic balance.

In a geostrophic eddy, the Coriolis force is balanced by the pressure gradient, and other forces are negligible. For some eddies, the combination of high rotational speeds and relatively short radii mean that centrifugal force is of the same order of magnitude as the other components. This cyclostrophic component, while negligible in most eddies, is responsible for most of the differences we see between the geostrophic assumption and the measured speeds, radii, and amplitudes in nonlinear eddies. $|\bar{\omega}/f|$ is the ratio of the magnitude of the cyclostrophic component u^2/R to the Coriolis component fu. If this ratio is very small, then the cyclostrophic component can be neglected and the eddy is in geostrophic balance; if it is not very small, this component of force must be included. This is referred to as the gradient wind balance. Thus, the distribution of $|\bar{\omega}/f|$ is an indication of how many eddies are influenced by cyclostrophic as well as geostrophic forces.

The distribution of $|\bar{\omega}/f|$ is shown in Figure 3d. The peak in the distribution of $|\bar{\omega}/f|$ is at 0.08. Seventy-five percent of eddy instances have $|\bar{\omega}/f|$ below 0.2 and 97% are below 0.5. This distribution gives a better

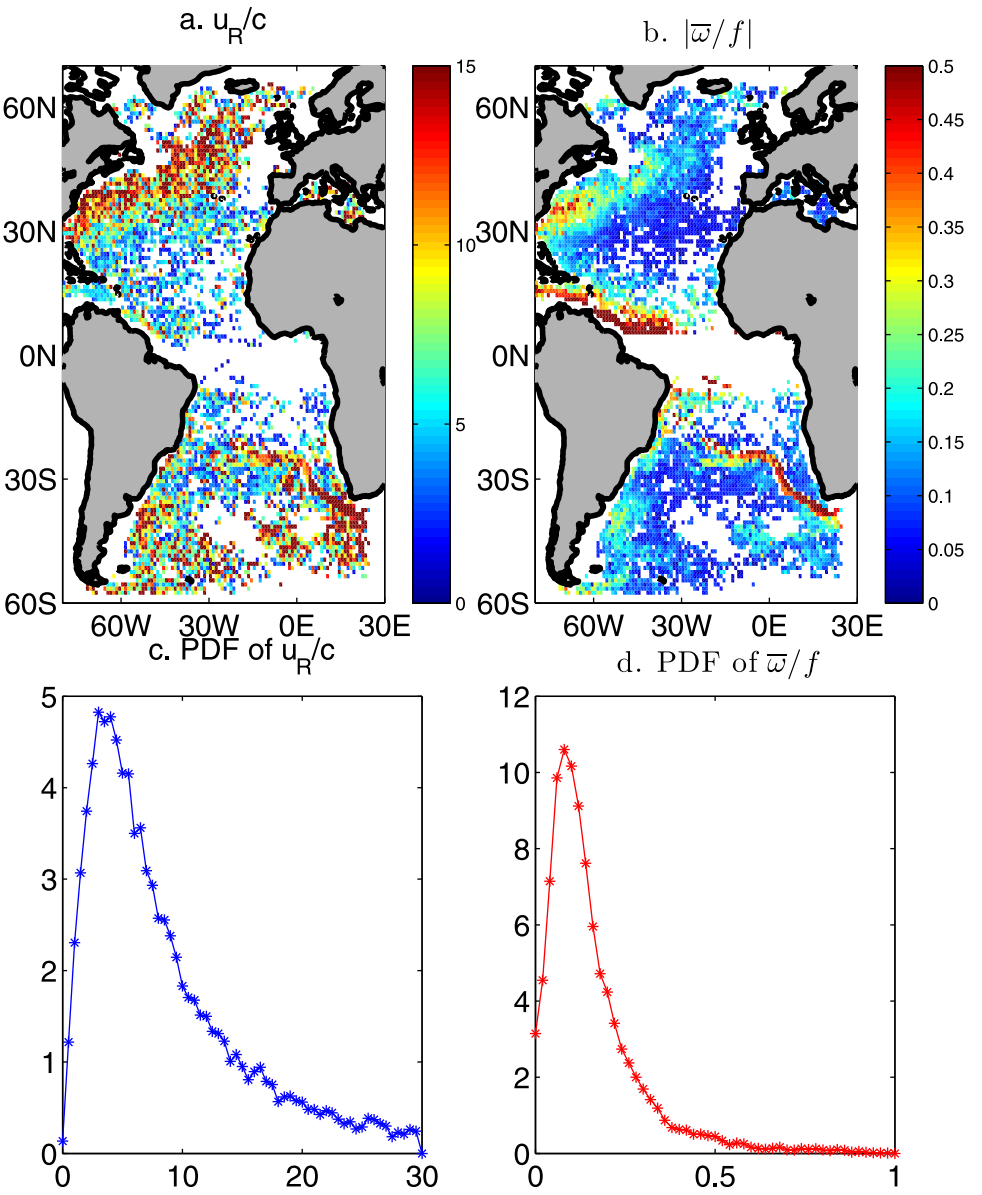

Figure 3. Distribution of nonlinearity parameters in the Atlantic. (a) Average u_R/c on a $1^\circ \times 1^\circ$. (b) Average $|\bar{\omega}/f|$ on a $1^\circ \times 1^\circ$ grid. (c) PDF of u_R/c. Bin widths are 0.5 (d) PDF of $|\bar{\omega}/f|$. Bin widths are 0.02.

metric for nonlinearity in the sense that the eddy's physical characteristics, and its dynamics, are not governed by the linear geostrophic assumption. For this reason, we choose $|\bar{\omega}/f| = Ro$ as the metric for "nonlinearity" in the remainder of this manuscript. As a threshold, we will define "strongly nonlinear" as those eddies with $Ro > 0.3$, or around 10% of eddy instances.

3.3. Anticyclonic Example

In the maps of nonlinearity, it is evident that there are certain regions with particularly high nonlinearity, including the Agulhas ring pathway and the Gulf Stream region. From those eddies with very high $|\bar{\omega}/f|$, two examples are chosen to illustrate the strong, nonlinear eddies we investigate in this manuscript.

The first example is a strong anticyclone. Agulhas rings are anticyclonic eddies that are "pinched off" south of Africa in the Agulhas retroflection region and travel northwestward across the Atlantic Ocean. These are long-lived warm core eddies, and are thought to transport heat, salt, and nutrients from the Indian Ocean

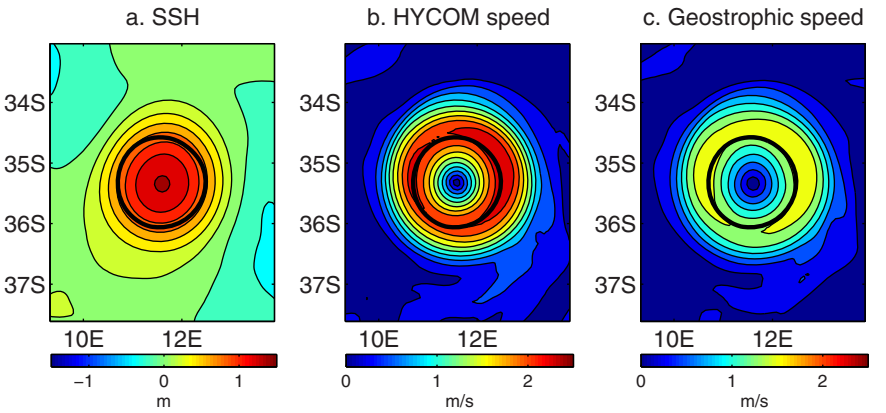

Figure 4. Demonstration of nonlinearity of anticyclonic eddy #18011, day 32, year 2003. This eddy has circularity of 0.99 and $|\bar{\omega}/f|$ of 0.68. (a) Contour plot of SSH, with W-contour in black to show the eddy border according to the OW algorithm. Units are m, contour interval is 0.20 m. (b) Contour plot of speed. Units are m/s, contour interval is 0.5 m/s. (c) As in Figure 4b, but for geostrophic speed. Geostrophy gives the correct structure of the speed field but significantly underestimates magnitude.

to the Atlantic. Figure 4 shows one of these Agulhas eddies. The sea surface height signature of the eddy, the rotational velocity from the HYCOM velocity fields, and the geostrophic velocity calculated from model SSH are all shown. The thick contour is the W-contour identified by the detection algorithm as the edge of the eddy. It is evident that the geostrophic velocity is considerably smaller than the rotational velocity estimated by the model. Geostrophic velocity around the contour is approximately 1.5 m/s, while the model velocity is approximately 2.3 m/s. $|\bar{\omega}/f|$ for this eddy is 0.68, in the top 2% of all values in the eddy field. This eddy has circularity of 0.99 and persists for 122 weeks. Its u_R/c is 19.2. It is clear that in this strongly nonlinear eddy, assuming sea surface height differences to be in geostrophic balance seriously underestimates rotational velocity.

3.4. Cyclonic Example

Strong cyclones also show a discrepancy, but in the opposite direction. For example, Figure 5 shows a cold-core eddy pinched off from the Gulf Stream. This eddy has rotational speed of 1.46 m/s, averaged around the W-contour, and a radius of 61 km. The geostrophic speed field has the same structure, but larger magnitude. Averaged around the W-contour, geostrophic speed is 1.85 m/s. $|\bar{\omega}/f|$ is 0.59, in the top 3% of all values in the eddy field. This eddy has circularity of 0.90, u_R/c of 109.2, and persists for 14 weeks. In this case, the rotational velocity is overestimated when geostrophic balance is used.

Each of these examples, the anticyclone and the cyclone, demonstrate that although the vast majority of ocean features are geostrophic, the assumption of geostrophic balance does not always hold in the case of the largest, strongest eddies.

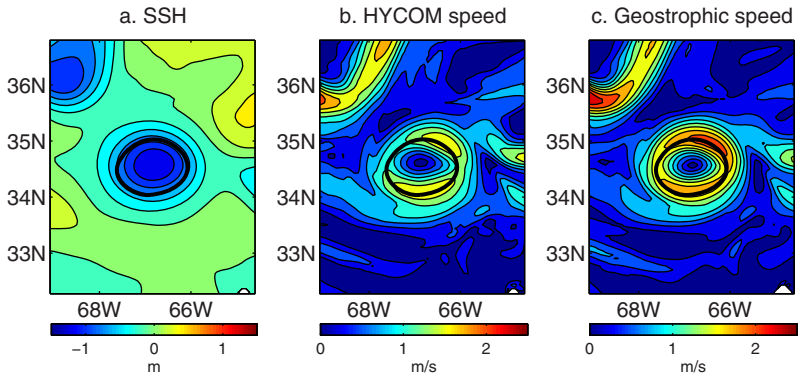

Figure 5. As Figure 4, but for cyclonic eddy #19452, day 172, year 2003. This eddy has circularity of 0.90 and $|\bar{\omega}/f|$ of 0.59. In the cyclonic case, geostrophy overestimates speed instead of underestimating it.

4. Balance of Forces

In the cases of strong eddies such as those shown in Figures 4 and 5, the assumption of geostrophy, which as noted is incorporated into the estimate of nominal amplitude, is not adequate to describe the forces at work on the eddy. In some of these cases, the centrifugal force generated from high rotational speed with a relatively small radius of curvature must be included. We will first demonstrate this balance of forces in an idealized case with a Gaussian-shaped eddy, and then show some examples of the force balance as calculated from the model fields.

4.1. Idealized Case

First, we consider an idealized case. With radius R_0 and nominal height η_0, the eddy height is:

$$\eta = \eta_0 e^{\frac{-r^2}{2R_0^2}} \tag{5}$$

For an anticyclone, where the centrifugal force balances adds to the pressure gradient force to balance the Coriolis force, the balance can be written as:

$$f_0 u_{gr} = g\frac{\partial \eta}{\partial r} + \frac{{u_{gr}}^2}{r} \tag{6}$$

where u_{gr} is the gradient rotational speed and u_g is the geostrophic speed. This quadratic equation for u_{gr} can be solved using the quadratic formula to give [*Knox and Ohmann*, 2006]:

$$u_{gr} = \frac{2u_g(r)}{1 \pm \sqrt{1 + (4u_g(r)/f_0 r)}} \tag{7}$$

where $u_g(r)$ is the geostrophic speed at radius r.

It is interesting to note that in equation (7), the effect on the eddy is associated with the sense of the eddy. In a cyclone, u_g and f will have the same sign, and u_{gr} will be less than u_g; in an anticyclone, u_g and f will have opposite signs, and u_{gr} will be greater than u_g. For anticyclonic features with large η_0 leading to large u_g, the sum under the square root sign can become negative as r gets close to zero. This effect was noted in *Penven et al.* [2014], who showed that for large η_0, the gradient wind equation has no solution for small radii. The fact that the solution only exists within a limited range should be taken into consideration when calculations are completed. In most cases, the solution is real at the radius R_0 located by the detection algorithm.

It must also be emphasized that this estimate of the gradient wind balance is only accurate in the case of axisymmetric, compact features. The detection algorithm requires eddies to be compact, and as noted, circularity is one of the measured attributes of each eddy. For highly circular eddies, the requirement of axisymmetry is generally met.

With this equation, we can solve for the gradient wind velocity of any eddy for which we have the geostrophic speed, radius, and latitude. The calculation of geostrophic speed must be done carefully, by calculating a full field of geostrophic velocity, and then finding the average geostrophic speed along the W-contour used to define the edge of the eddy.

4.2. Example Force Balances

As an example of the importance of the cyclostrophic term, all three components of the balance of forces are shown for eddy #18011 on day 32 of year 2003 in Figure 6. Note that this is the same eddy used to demonstrate nonlinearity in Figure 4. This is a very strong, distinct Agulhas ring. In the diagram, positive terms indicate a force directed outward from the eddy center, and negative forces are directed inward. As this eddy is an anticyclone, the pressure gradient force and cyclostrophic term combine to oppose the Coriolis force. The HYCOM velocity and geostrophic velocity fields from Figure 4 are shown again, as well as the u_{gr} field calculated using equation (7). The eddy is highly circular, and the gradient wind speed shown in Figure 6f is a good approximation of HYCOM rotational speed. The cyclostrophic force term, while smaller than the other two (note the color bars), is still significant enough to have a clear effect. Note also that close to the center, when r is small, u_{gr} becomes imaginary, but at R_0, the solution is real.

In this example, the Coriolis force averaged along R_0 is -10.1×10^{-5} m s^{-2}. The pressure gradient force along that same contour is 5.2×10^{-5} m s^{-2}, and the cyclostrophic term is 4.3×10^{-5} m s^{-2}. The residual

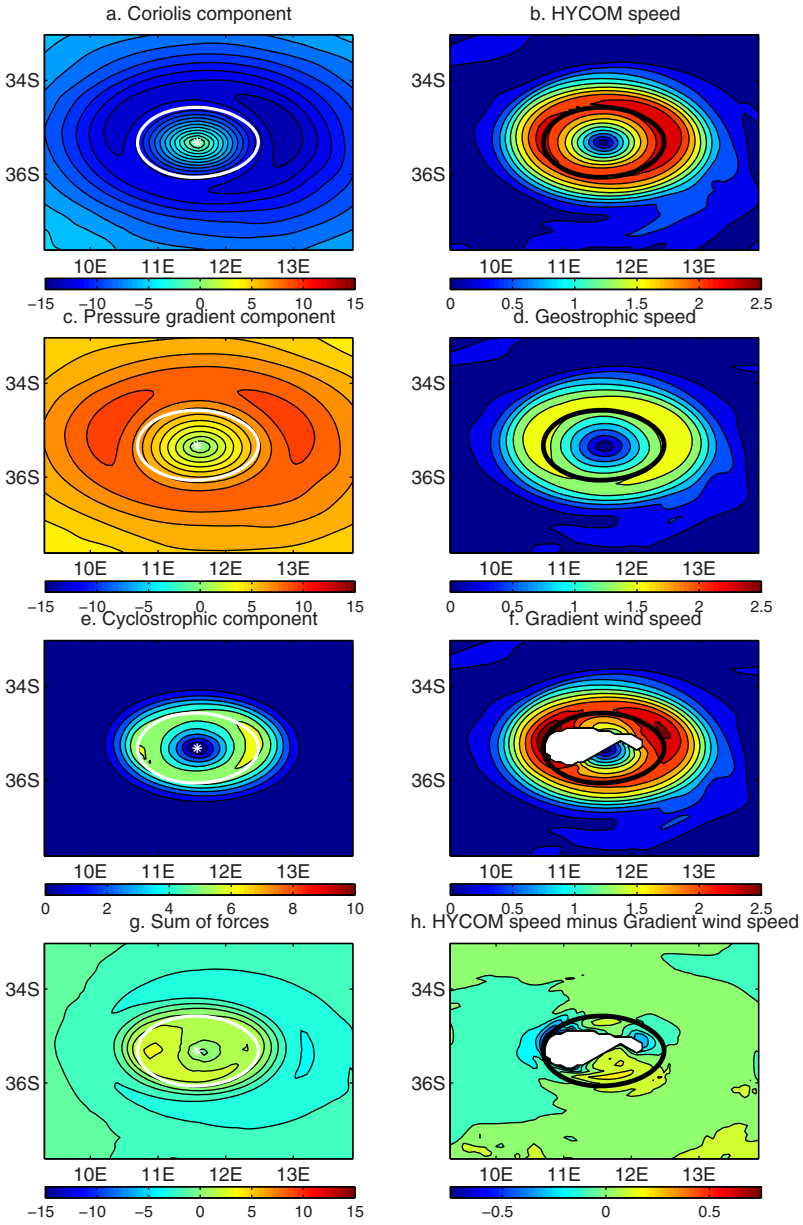

Figure 6. Components of force balance on eddy #18011, day 32, year 2003. Units for (a), (c), (e), and (g) are 10^{-5} m s^{-2}. Positive values indicate force directed outward from eddy center. Units for (b), (d), (f), and (h) are (m/s). (a) Coriolis force. (b) Hycom speed field. (c) Pressure gradient force. (d) Geostrophic speed. (e) Cyclostrophic force. (f) Speed calculated using gradient wind balance. Note that gradient wind velocity is undefined close to eddy center. (g) Sum of forces (a + c + e). (h) Hycom speed minus gradient wind speed (Figures 6b–6f).

force, averaged along R_0, is -1.3×10^{-5} m s^{-2}. The cyclostrophic term is 40% of the dominant (Coriolis) term, while the residual is only 13% of the dominant term.

Figure 7 shows the force balance of a cold-core ring, the same eddy shown in Figure 5. Note that the directions of the Coriolis and pressure gradient terms are reversed from the anticyclonic case, but the cyclostrophic component is always directed outward. As with the anticyclone in Figure 6, the cyclostrophic term must be included to find a balance of forces.

For the cyclone, the Coriolis force of 4.3×10^{-5} m s^{-2} is nearly balanced by the pressure gradient force of -4.9×10^{-5} m s^{-2}. Inclusion of the cyclostrophic term of 1.2×10^{-5} m s^{-2} moves the system even closer to being balanced. The contour-averaged residual in this case is 0.58×10^{-5} m s^{-2}. Here the magnitude of

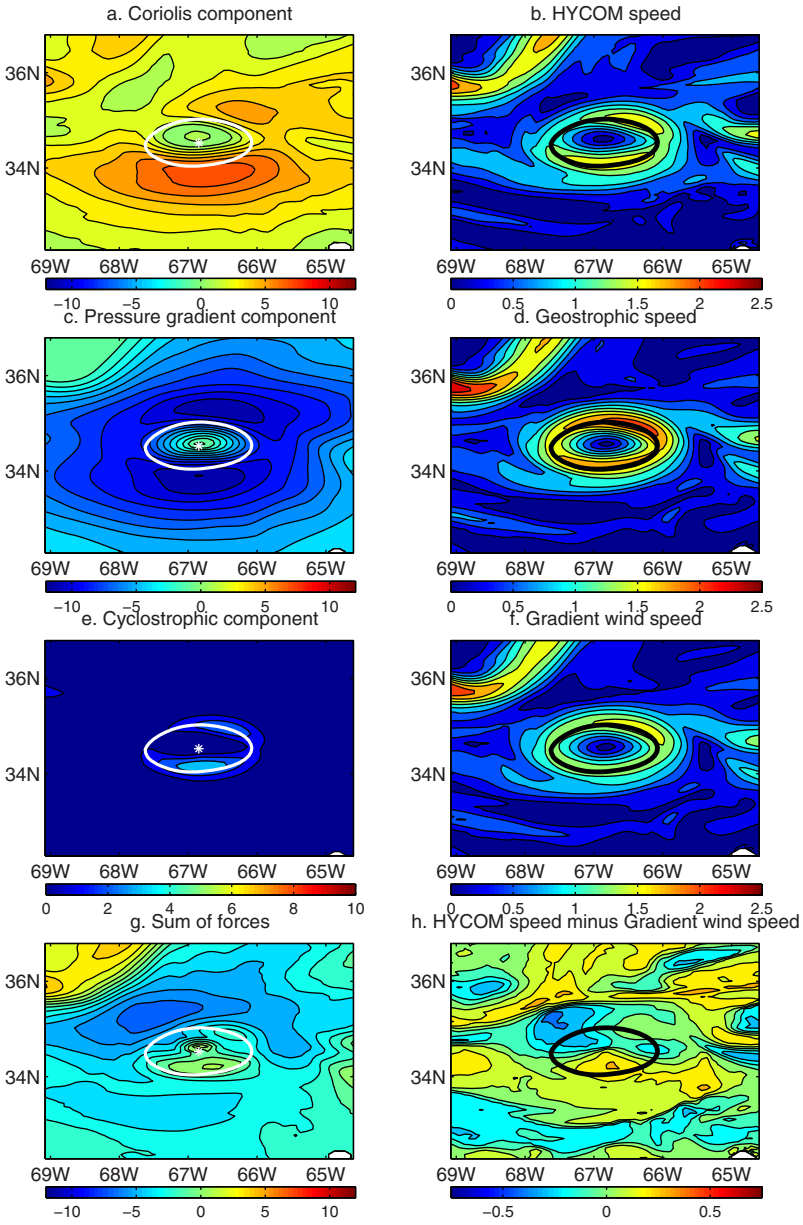

Figure 7. As Figure 6, for eddy #19452 on day 172 of 2003. Note that directions of PGF and Coriolis forces are reversed for this cyclone, but the cyclostrophic component is still directed outward.

the cyclostrophic term is 24% of the dominant (pressure gradient) term, while the residual is 12% of that term. Note that the Coriolis term is dominant in anticyclones, while the pressure gradient term dominates in cyclones.

4.3. Residuals

Determining the force balance along the W-contour is a noisy calculation. *W*, calculated from the derivative of velocity, is a noisy field to begin with. Imbalances can be introduced from nearby eddies, currents, or transient features. In less circular eddies, additional error is introduced, due to the assumption of axisymmetry inherent in the calculation of the gradient wind balance. On average, the magnitude of the residual is 25% of the dominant term, with a standard deviation of 31%. The cyclostrophic term is relatively small in comparison. Its magnitude is 8% of the dominant term, with standard deviation of 8%. But in eddy instances defined as strong (see section 5), the magnitude of the cyclostrophic term is 21% of the dominant term, while the residual is only 16%. In these strong eddies, the cyclostrophic term is clearly more important.

Although it is smaller in magnitude, inclusion of the cyclostrophic term does improve the estimate of the balance of forces most of the time. In 56% of eddy instances, residuals from the force balance of Coriolis plus pressure gradient plus cyclostrophic are smaller than those from Coriolis plus pressure gradient alone. Among strong eddies, 79% have smaller residuals when the cyclostrophic term is included.

5. Determination Criteria

We have demonstrated that in some circumstances, the cyclostrophic force is important enough to disrupt characterization of eddies using only geostrophy. The question is, what criteria can we use to determine the importance of this term?

The first criteria we include are a high Rossby number. As discussed in the previous section, the Rossby number is a measure of the nonlinearity of an eddy. If we consider the gradient wind balance, the cyclostrophic term is scaled like the Rossby number; if this value is of the order of 1, then the cyclostrophic term is of the same order as the pressure gradient and geostrophic terms. In these cases, this term should not be omitted. As mentioned previously, the threshold is set at $Ro > 0.3$. Twelve percent of the eddies meet this criteria.

The second criteria are high circularity. The idealized equations are derived on the basis of an eddy that is precisely circular, and the gradient wind equation as stated is valid in the case of an axisymmetric system. Our examples show that highly compact, intense eddies are quite circular; the loss of that circularity implies that either the eddy is being impacted and distorted by external forces (which would disrupt the gradient wind balance), or that some other process such as an eddy splitting into two or merging with another eddy is at play. In either case, the gradient wind balance would not be an accurate description of the system. Thus, we require eddies to have a circularity of at least 0.89, which is the median value of circularity of identified features; by definition, 50% of eddies meet this criteria.

The final criteria we include in our selection of these eddies are latitude. Eddies close to the equator have very small values of the Coriolis parameter f, which leads to high Rossby number. Although some of these eddies are also highly circular, most of them have very small amplitudes. We will only consider eddies found more than 10° from the equator.

These three criteria will ensure that the eddies we consider are truly "strong" eddies in our eddy field. Their distribution can enlighten us as to where we will expect to find such eddies, and what they might look like if only their sea surface height, for example, were visible to us. This will assist us in identifying and characterizing such eddies in observations.

5.1. "Strong Eddy" Characteristics

Recall that in order to estimate eddy amplitude using the OW algorithm for eddy detection, given the rotational velocity and radius, the assumptions of geostrophy and Gaussian shape were introduced. For these very strong, nonlinear eddies, these assumptions may be revisited. The SSH profiles of the strong anticyclone and cyclone introduced earlier, along with the Gaussian approximations estimated from rotational velocity and radius, are shown in Figure 8. In each figure, the Gaussian estimate intersects the cross section at $R = R_0$. In Figure 8a, the strong anticyclone, the Gaussian amplitude is considerably larger than the actual change in SSH. The Coriolis force on anticyclone in gradient wind balance is opposed by both the pressure gradient force and the centrifugal force, so a smaller height gradient is present than if the Coriolis force were opposed by the pressure gradient force alone. The converse is shown in Figure 8b, in which a cyclonic eddy is shown to have a greater amplitude than the Gaussian estimate resulting from the rotational velocity and radius associated with it. In the cyclonic system, the Coriolis force and centrifugal force combine to oppose the pressure gradient force, so the pressure gradient is larger than in a system where the centrifugal force is negligible.

The examples show the distinct difference between measured amplitude and predicted amplitude in "strong eddies." Comparing these quantities will both demonstrate the magnitude of the effect of the gradient wind balance, and allow us to evaluate the criteria for "strong eddies." For each eddy, the measured amplitude (ΔSSH) is the difference between the enclosed SSH extremum and the SSH at the encircling

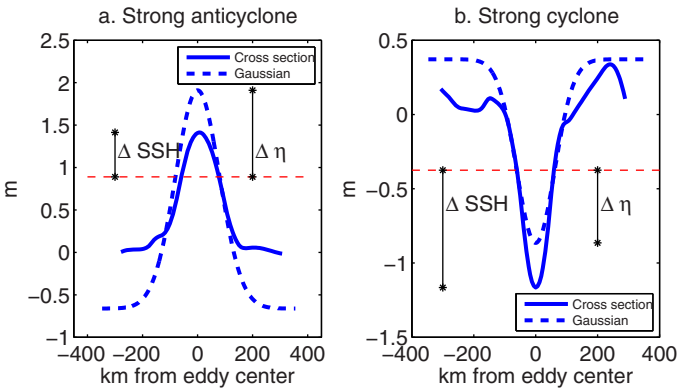

Figure 8. (a) Cross section of sea surface height from a strong anticyclone, along with the associated Gaussian. The two profiles intersect at the point of the eddy border (at $r = R_0$). The amplitude differences ΔSSH and $\Delta\eta$ are also shown. In an anticyclone, $\Delta\eta$ exceeds ΔSSH: amplitude is overestimated. (b) As Figure 8a, but for a strong cyclone. In a cyclone, $\Delta\eta$ is smaller than ΔSSH: amplitude is underestimated.

contour. The predicted amplitude, in a Gaussian, geostrophic eddy, is the difference between η at $r = 0$ and η at $r = R_0$ is $\Delta\eta = \eta_0(1 - e^{-1/2})$. Both ΔSSH and $\Delta\eta$ are shown in Figure 8.

For each eddy instance, ΔSSH and $\Delta\eta$ are plotted against each other in Figure 9. The green line in Figure 9b is the 1:1 line, plotted for reference. The points circled in red are "strong" anticyclones, while those circled in cyan are "strong" cyclones. The anticyclones stand out, with extremely high magnitudes and a clear linear relationship between geostrophic and measured amplitude. It is also clear that most of the eddy instances along the red line are circled in red, indicating that our selection criteria capture most of the anomalously strong anticyclonic instances. In the gradient wind balance, geostrophy will over predict amplitude in a strong anticyclone and under predict amplitude in a strong cyclone. Accordingly, the cyan dots are mostly above the 1:1 line, and anticyclones are mostly below the same line. This also indicates that the selection criteria are reasonable.

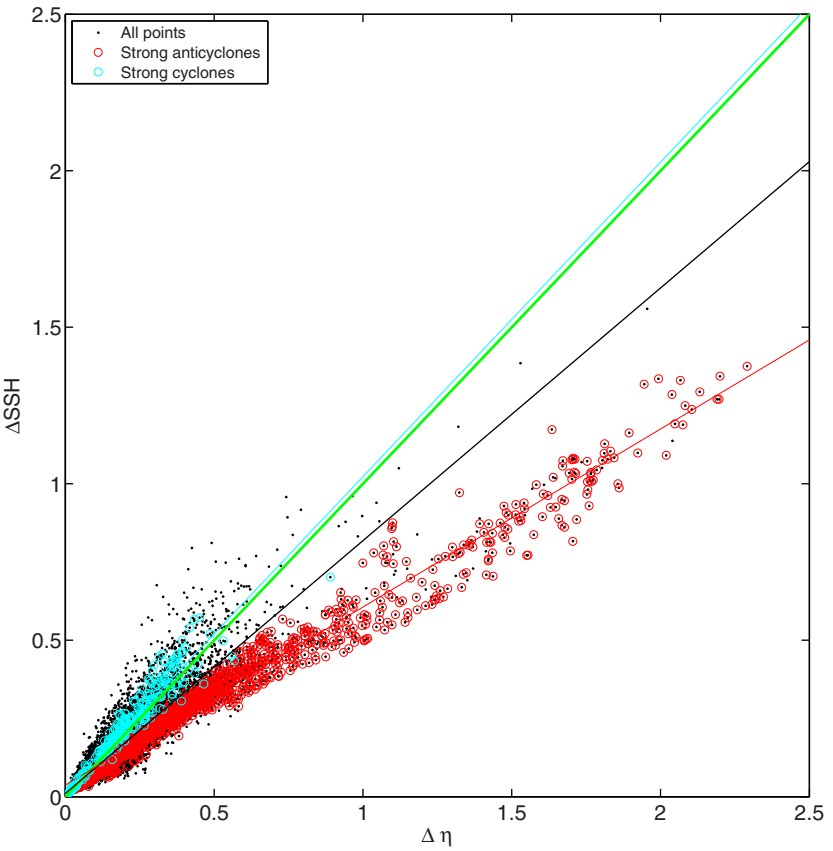

Figure 9. ΔSSH plotted against $\Delta\eta$, along with best fit lines for strong anticyclones (red), strong cyclones (cyan), and the rest of the eddies (black). The green line is the 1:1 line for comparison.

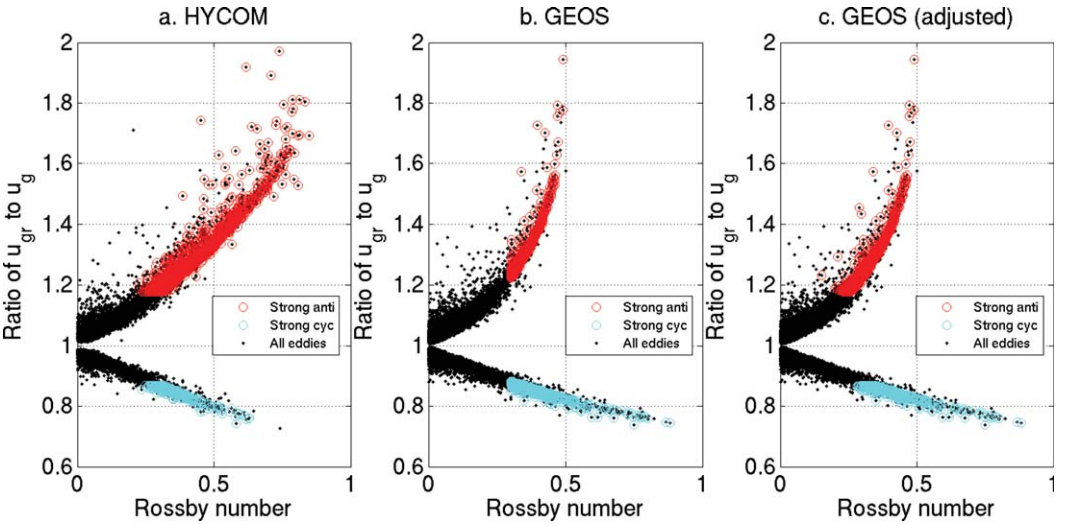

Figure 10. (a) Plot of the Rossby number as a function of the ratio of gradient wind speed to geostrophic speed in HYCOM eddy census. Strong anticyclones are highlighted in red, strong cyclones in cyan. (b) As Figure 10a, but for GEOS. Rossby numbers are higher in HYCOM than in GEOS. (c) As Figure 10b, but with strong eddies determined by Rossby number from the gradient wind speed. GEOS has more strong anticyclones and fewer strong cyclones.

A linear fit was performed to each collection of points: the strong anticyclones, the strong cyclones, and the remainder. The measured amplitude of strong anticyclones (6.7% of instances) is 0.57 times the predicted amplitude of a Gaussian eddy in geostrophic balance (red line). The measured amplitude of strong cyclones (1.3% of instances) is 1.00 times the predicted amplitude of Gaussian cyclones in geostrophic balance (cyan line). On average, the measured amplitude of an eddy not identified as strong is 0.81 times the predicted amplitude (black line). Thus, the Gaussian approximation tends to slightly overpredict amplitude, but the effect of the gradient wind balance on those eddies with high Rossby number and circularity is clearly discernible. It is noteworthy that these strongly nonlinear, highly circular eddies make up less than 10% of instances: in most cases, the estimate of a Gaussian eddy in geostrophic balance is reasonable.

Another way to look at the effect of the gradient wind balance is to calculate, using equation (6), the predicted rotational speed including the cyclostrophic term. In most eddies, the cyclostrophic term will be quite small and the predicted rotational speed will only differ slightly from the actual rotational speed. Figure 10a shows the ratio of u_{gr} to u_g for all eddies, plotted against the magnitude of the Rossby number. Seventy percent of eddies have gradient wind speed between 90% and 110% of their geostrophic speed. Some of the deviation from $u_{gr} = u_g$ at very small Rossby number is due to very small values for both u_{gr} and u_g. However, as the Rossby number increases, the difference between u_{gr} and u_g is systematic. The cutoff of 0.3 as the Rossby number of interest means that the weakest of the strong anticyclones has a gradient wind speed that is 115% of its geostrophic wind speed, and the weakest of the strong cyclones has a gradient wind speed that is 88% of its geostrophic wind speed. The ratio increases consistently with Rossby number for anticyclones, and decreases consistently for cyclones.

6. Detection in Geostrophic Maps

This analysis was performed on a velocity field from a model which includes all nonlinear terms. However, it would be useful to be able to identify nonlinear eddies from sea surface height alone, since satellite altimetry is readily available on a global scale. In this case, only geostrophic velocities are available. Because the gradient wind velocity can be calculated with knowledge of the geostrophic velocity, the eddy radius, and the latitude, it is possible that the same analysis could provide useful insight into which eddies identified by satellite altimetry might have stronger rotational velocities than simple geostrophic calculations would project.

To test this hypothesis, geostrophic velocity fields were calculated from the model SSH, and the eddy detection algorithm was applied. This estimate of the eddy field will be referred to hereafter as GEOS, while the

Table 1. Number of Strong Identified Features Found in Both the HYCOM and the GEOS Eddy Fields[a]

	HYCOM Found Strong	HYCOM Found Not Strong	HYCOM Not Found
GEOS found strong Rossby from u_g	1029	249	243
GEOS found not strong Rossby from u_g	741		
GEOS not found Rossby from u_g	243		
GEOS found strong Rossby from u_{gr}	1455	194	251
GEOS found not strong Rossby from u_{gr}	315		
GEOS not found Rossby from u_{gr}	116		

[a]Only features identified as "strong" in one or the other field are considered.

original eddy field estimate will be referred to as HYCOM. There are some differences between the overall descriptions of the eddy fields. Overall, more eddies are detected in the GEOS maps (47836) than in the HYCOM maps (23503). On average, the eddies in the GEOS field have smaller amplitudes, shorter radii, and slower rotational speeds. These differences are likely due to large-scale nonlinear flows, such as Ekman transport, which affect the surface velocities in the fully nonlinear HYCOM field, but would be undetected by geostrophy. Since one of the criteria for eddy detection is vorticity exceeding shear (in the OW algorithm) or flow in the northern, southern, eastern, and western directions (in the SSH algorithm), a large-scale background flow such as this would smooth over small "bumps" of sea surface height. As a result, these small "bumps" in sea surface height are identified as eddies in the GEOS maps, but not in the HYCOM maps, accounting for the large differences in the number of eddies detected. Although the average eddy descriptions are affected, particularly strong eddies are still likely to be well defined in both the HYCOM and GEOS maps.

Using the criteria of Rossby number greater than 0.3 and circularity higher than 0.89, 1521 strong eddy instances were identified in GEOS: 791 strong anticyclones and 730 strong cyclones. The total number is similar to the 1886 strong eddy instances found in HYCOM; however, HYCOM has more anticyclones (1576) and fewer cyclones (310). Of these eddy instances, 1029 were identified as strong in both fields: 746 anticyclones and 283 cyclones. So most of the strong eddies were common to both fields.

Of eddy instances identified in both fields, there were 741 eddy instances identified as strong in HYCOM but not GEOS, and 116 instances that were strong in HYCOM but not identified in GEOS at all. There were 249 eddy instances identified as strong in GEOS but not HYCOM, and 243 instances identified as strong in GEOS and not found at all in HYCOM (Table 1). To understand these differences, it is important to recall that these are snapshots. As such, differences in eddy strength could indicate that the rotational speed of an eddy is slightly different and the Rossby number drops below the threshold for identification as "strong." Most of these discrepancies occur in the Gulf Stream region, where there are many eddies and interactions which could affect eddy detection or the eddy characteristics.

When cyclonicity of these differences is considered, there is a strong bias. Of the 857 eddy instances identified as strong in HYCOM and either weak or not found in GEOS, 830 are anticyclones. This indicates an underdetection of strong anticyclones in the GEOS maps. Of the 492 eddy instances identified as strong in GEOS and either weak or not found in HYCOM, 447 are cyclones. Thus, strong cyclones are overdetected in the GEOS maps. This bias is related to the differences between the geostrophic speed and the gradient wind speed in strong eddies. In the GEOS field, all velocities are geostrophic. In strong anticyclones, the geostrophic speed is smaller than the actual rotational speed, which can be estimated from the gradient wind speed. The underestimation of speed leads to underestimation of Rossby numbers in anticyclones, which in turn leads to a smaller number of eddy instances identified as "strong." The converse is true in cyclones, where the geostrophic speed is higher than the actual rotational speed, leading to high Rossby numbers and more cyclones described as "strong" than is accurate.

To alleviate this problem, we calculated the gradient wind speed in all eddy instances. The Rossby number can then be determined based on the gradient wind velocity. Using this "adjusted" Rossby number, 1900 strong eddy instances were identified in GEOS: 1328 strong anticyclones and 572 strong cyclones. Of these eddy instances, 1455 were also identified as strong in HYCOM: 1175 anticyclones and 280 cyclones. More strong eddies were identified in GEOS, and the proportion of strong anticyclones to strong cyclones agrees

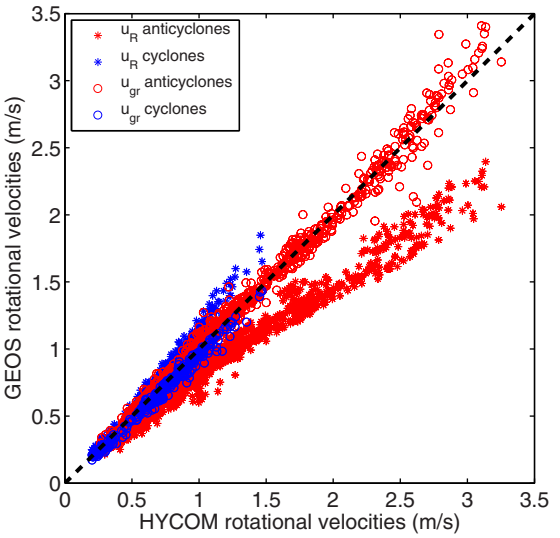

Figure 11. Comparison of velocities for strong eddies found in both HYCOM and GEOS. While geostrophic rotational velocities are biased according to their sense of rotation, the gradient wind estimates of rotational speed are very good matches for the velocities from the HYCOM fully nonlinear velocity field.

much more closely with the fully nonlinear field. Additionally, there is a significant increase in the number of strong eddy instances found and identified as strong in both HYCOM and GEOS.

With the adjustment to GEOS, there were 315 eddy instances identified as strong in HYCOM but not GEOS, and 194 eddy instances identified as strong in GEOS but not HYCOM (Table 1). There were also 116 strong HYCOM eddies that were not identified in GEOS at all, and 251 eddies identified as strong in GEOS and not found at all in HYCOM. The number of eddies listed as strong in one field and not the other increased slightly.

The bias in cyclonicity is still present. Of 431 eddy instances identified as strong in HYCOM and either weak or not present in GEOS, 401 are anticyclonic. Of 445 eddy instances identified as strong in GEOS and either weak or not present in HYCOM, 292 are cyclones. The number of eddies that are detected in one field is smaller than when the geostrophic speed was used instead of the gradient wind speed, and the bias is not as strong, but it is still evident that relative to the HYCOM maps, GEOS maps are biased away from anticyclones and toward cyclones.

The increasing ratio of u_{gr} to u_g as a function of Rossby number is shown for GEOS in Figure 10b. Just as in HYCOM, higher Rossby numbers are associated with higher ratios. Rossby numbers for anticyclones in GEOS tend to be lower (the maximum is 0.5, rather than 0.8 for HYCOM), because velocities are lower and Rossby number is directly proportional to velocity. To see where the "extra" strong anticyclones are coming from, when the adjusted Rossby number is used to identify strong eddy instances, Figure 10c shows the same values as Figure 10b, colored with the strong identifications from the adjusted Rossby number. The biggest difference comes in anticyclones whose unadjusted Rossby number is just below 0.3. More of these eddy instances are now identified as strong. "Strong" anticyclones are now those with a ratio of u_{gr} to u_g of greater than about 1.18. This is similar to HYCOM (Figure 10a). Since these eddy instances are clearly affected by the use of gradient wind speed, the "strong" label seems appropriate.

For all strong eddies found by both HYCOM and GEOS, HYCOM rotational speeds are plotted against the GEOS rotational speeds in Figure 11. For anticyclones (red stars), the HYCOM estimate exceeds the GEOS estimate, and for cyclones (blue stars), the HYCOM estimate of rotational speed is lower than GEOS. However, when the gradient wind speeds from GEOS are plotted against HYCOM rotational speeds, the biases disappear, regardless of sense of rotation (red and blue circles). This demonstrates that the gradient wind balance recovers the nonlinear HYCOM rotational speeds from the geostrophic velocities.

The estimates of other eddy properties also are affected by the assumption of geostrophy in the construction of the GEOS velocity field. Since the eddy shape is different when the cyclostrophic term is important, the detection of radius and estimate of nominal amplitude are affected as well. A strong anticyclone in GEOS has a radius that averages 5.9 km larger, with a standard deviation of 5.6 km, than its counterpart in the fully nonlinear HYCOM velocity field. Nominal amplitudes from GEOS average 13 cm smaller than HYCOM amplitudes, but the standard deviation of the difference is 24 cm, so these differences are not statistically significant. Overall, these biases are minor. The plots of radius and nominal amplitude for eddies found by both algorithms are shown in

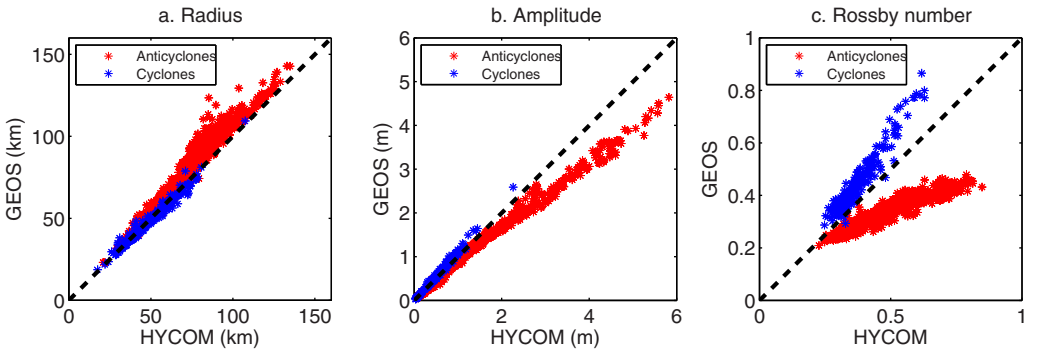

Figure 12. Comparison of properties for strong eddies found in both HYCOM and GEOS. (a) Radius; (b) Amplitude; (c) Rossby number. Nominal amplitudes and Rossby numbers of strong eddies are systematically affected by nonlinearity in the HYCOM field.

Figures 12a and 12b. The Rossby number (Figure 12c) has more significant bias, as it is directly proportional to velocity.

7. Altimetric Maps

While we have presented an analysis based on model velocity and SSH, this method is applicable to altimetric maps as well. Maps of satellite altimetry are available from Archiving, Validation, and Interpretation of Satellite Oceanographic data (AVISO). AVISO uses objective analysis to create maps of SSH every 7 days with horizontal resolution of 1/3°. The eddy detection algorithm was applied to 3 years of output, from October 2002 and September 2005. During this time period, data from four satellites (Topex/Poseidon, GFO, Envisat, and Jason-1) were available.

Overall, the eddy detection algorithm locates approximately twice as many eddies in the altimetric maps (54300) as in the model product (23053). There are several relevant statistical differences between the altimetric eddy field and that from the model output. First of all, circularity is lower in the altimetric product. The median circularity is 0.82 rather than 0.89 in the HYCOM field. Eddies are required to have circularity higher than the median to be considered strong.

Additionally, the rotational speeds are significantly lower in the AVISO field. This is reflected in lower vorticity and lower Rossby number. As a result, far fewer eddies are identified as "strong" in the altimetric maps, than were identified in the model output.

Using the "adjusted" Rossby number calculated from the gradient wind velocity, only 81 eddy instances in 3 years of AVISO output are identified as strong. Thirty one of these are anticyclones, and 50 are cyclones. It is noteworthy that only one of the anticyclones is an Agulhas ring, while in the model output, Agulhas rings made up the majority of the very strong, nonlinear anticyclones. Examination of AVISO maps shows that while Agulhas rings are present in the output, their amplitudes are significantly smaller than the amplitudes of Agulhas rings in the model output. Snapshots of the Agulhas region on the day when the strongly nonlinear anticyclone is identified in AVISO, and on the same date in the HYCOM model, show that Agulhas rings are significantly larger in amplitude and radius, and are traveling on a very distinct pathway in the model (Figure 13). In the altimetric map, the eddy field appears more turbulent and eddies are less well defined. The issue of Agulhas eddies traveling along a path that is too well defined has been previously noted in HYCOM as well as in other general circulation models [*McClean et al*., 2011]. While the HYCOM estimate presented in this manuscript may overestimate the number and magnitude of Agulhas rings, the analysis of the physics of the rings is still valid.

8. Summary and Conclusions

This analysis explores characteristics of very strong, nonlinear surface eddies in the Atlantic Ocean. The eddies are detected in the fully nonlinear velocity field from the HYCOM model output from October 2002 to September 2005. The detection algorithm requires that each eddy has both vorticity and SSH signatures, so a robust eddy field is obtained. About 8% of eddy instances cannot be correctly characterized by

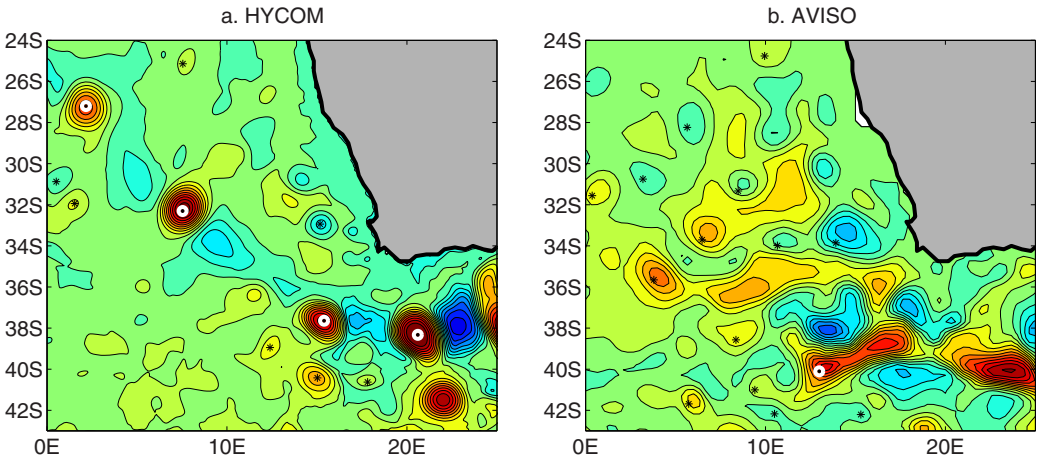

Figure 13. Maps of sea surface height in (a) HYCOM and (b) AVISO. Black asterisks indicate eddies, and white circles indicate strong eddies. The Agulhas rings in the model are much more distinct and have much larger amplitude than those in the altimetric maps.

geostrophic balance. The combination of high rotational speed and short radius lead to a centrifugal force of the same order of magnitude as the Coriolis and pressure gradient forces, which must be accounted for when describing these eddies.

Examples of these eddies include cold-core Gulf Stream rings and Agulhas rings. While Agulhas rings are only a small percentage of total eddies in the Atlantic, they are thought to be important players in the transport of warm salty water to from the Indian Ocean toward the equatorial Atlantic. Their ability to transport water effectively without mixing is a reflection of their nonlinearity.

The Rossby number provides a useful measure of nonlinearity of eddies. Those eddies that have high Rossby number as well as high circularity are identified as "strong" eddies. These eddies are found to have longer lifetimes on average than other eddies. When geostrophy is used to estimate the nominal amplitudes of these eddies from their radius and rotational speed, the amplitudes of anticyclones are seriously overestimated, while cyclones are underestimated. Conversely, using geostrophy to estimate the rotational velocity from sea surface height provides results that are inconsistent with the model velocity field.

The rotational speed of an eddy in gradient wind balance, rather then geostrophic balance, can be calculated analytically from the geostrophic rotational velocity and the eddy radius. The magnitude of the change in velocity resulting from this correction increases with the Rossby number. The adjustment is only significant in about 7% of anticyclones and less than 1.5% of cyclones. Since those eddies are the strongest eddies, and as a result are the most likely to be involved in cross-basin transport of nutrients (in the case of Agulhas rings, in particular), it is important to characterize them properly.

These nonlinear eddies can be characterized properly even when only the linear geostrophic velocity field is available. Since the gradient wind speed is calculated from geostrophic velocity, along with the radius and latitude, it can be calculated for any eddy. Comparisons between the eddy field as determined from a linear geostrophic field and the eddy field from the fully nonlinear field shows that approximately the same number of strong eddies are found, with a similar breakdown between anticyclones and cyclones. Gradient wind speeds can be calculated from geostrophic velocities that are nearly equal to the speeds found directly from nonlinear model fields. Only minor biases are evident in estimates of radius and amplitude. Thus, even when only linear geostrophic velocities are available, the gradient wind calculation should be used in cases of high Rossby number and high circularity, to correctly characterize the rotational speed of strongly nonlinear eddies.

Applying these principles to an eddy census from AVISO altimetric maps shows that such strongly nonlinear eddies are less prevalent in the satellite observations than in the model. However, some of these eddies do exist, and this analysis allows us to characterize their rotational speeds correctly for a better understanding of their dynamics.

Acknowledgments
The data used in this manuscript include output from HYCOM version 10.2 run by the Naval Research Laboratory. We are in the process of making this model run available on the www.hycom.org data server. We also used the delayed-time multimission gridded altimetry product from AVISO, available at www.aviso.altimetry.fr, downloaded on 20 July 2008. We acknowledge support by the projects "Eddy resolving global ocean prediction including tides," "Ageostrophic vorticity dynamics," and "Earth Systems Prediction Capability," all sponsored by the Office of Naval Research.

References

Bleck, R. (2002), An oceanic general circulation model framed in hybrid isopycnic-Cartesian coordinates, *Ocean Modell.*, *4*(1), 55–88.
Chassignet, E. P., L. T. Smith, G. R. Halliwell, and R. Bleck (2003), North Atlantic simulations with the Hybrid Coordinate Ocean Model (HYCOM): Impact of the vertical coordinate choice, reference pressure, and thermobaricity, *J. Phys. Oceanogr.*, *33*(12), 2504–2526.
Chelton, D. B., M. G. Schlax, and R. M. Samelson (2011), Global observations of nonlinear mesoscale eddies, *Prog. Oceanogr.*, *91*(2), 167–216.
Halliwell, G. R. (2004), Evaluation of vertical coordinate and vertical mixing algorithms in the HYbrid-Coordinate Ocean Model (HYCOM), *Ocean Modell.*, *7*(3–4), 285–322.
Isern-Fontanet, J., E. García-Ladona, and J. Font (2003), Identification of marine eddies from altimetric maps, *J. Atmos. Oceanic Technol.*, *20*(5), 772–778.
Knox, J. A., and P. R. Ohmann (2006), Iterative solutions of the gradient wind equation, *Comput. Geosci.*, *32*(5), 656–662.
McClean, J. L., et al. (2011), A prototype two-decade fully-coupled fine-resolution CCSM simulation, *Ocean Modell.*, *39*(1–2), 10–30.
Metzger, E. J., H. E. Hurlburt, X. Xu, J. F. Shriver, A. L. Gordon, J. Sprintall, R. D. Susanto, and H. M. van Aken (2010), Simulated and observed circulation in the Indonesian Seas: 1/12° global HYCOM and the INSTANT observations, *Dyn. Atmos. Oceans*, *50*(2), 275–300.
Penven, P., I. Halo, S. Pous, and L. Marié (2014), Cyclogeostrophic balance in the Mozambique Channel, *J. Geophys. Res. Oceans*, *119*, 1054–1067, doi:10.1002/2013JC009528.
Saha, S., et al. (2010), The NCEP climate forecast system reanalysis, *Bull. Am. Meteorol. Soc.*, *91*(8), 1015–1057.